Scalable, large area compound array refractive lens for hard X-rays

Stefan Reich,[1] Tomy dos Santos Rolo,[1] Alexander Letzel,[2] Tilo Baumbach,[1,3] and Anton Plech[1,a)]

[1)] *Karlsruhe Institute of Technology (KIT), Institute for Photon Science and Synchrotron Radiation (IPS), Herrmann-von-Helmholtz-Platz 1, 76344 Eggenstein-Leopoldshafen, Germany.*

[2)] *University of Duisburg-Essen, Technical Chemistry I and Center for Nanointegration Duisburg-Essen (CENIDE), Universitätsstrasse 7, 45141 Essen, Germany.*

[3)] *Karlsruhe Institute of Technology (KIT), Laboratory for Applications of Synchrotron Radiation (LAS), Engesserstrasse 15, 76131 Karlsruhe, Germany.*

(Dated: 28 March 2018)

We demonstrate the fabrication of a 2D Compound Array Refractive Lens (CARL) for multi-contrast X-ray imaging. The CARL consists of six stacked polyimide foils with each displaying a 2D array of lenses with a 65 µm pitch aiming for a sensitivity on sub-micrometer structures with a (few-)micrometer resolution in sensing through phase and scattering contrast at multiple keV. The parabolic lenses are formed by indents in the foils by a paraboloid needle. The ability for fast single-exposure multi-contrast imaging is demonstrated by filming the kinetics of pulsed laser ablation in liquid. The three contrast channels: absorption, differential phase and scattering are imaged with a time resolution of 25 µs. By changing the sample-detector distance it is possible to distinguish between nanoparticles and microbubbles, respectively.

Keywords: laser ablation in liquids, multi contrast retrieval, scattering contrast imaging, X-ray lens.

X-ray absorption radiography is a widely used technique for non-destructive imaging of strongly attenuating samples. For imaging samples with low absorption, the phase and scattering (dark-field) contrast can be exploited to obtain additional information[1–4]. A recent approach to obtain all three contrast types with a single experimental setup is to employ grating interferometry (GI). Here the X-ray beam is analyzed via a set of gratings by means of the Talbot self-imaging effect after being perturbed by the specimen under investigation[5]. However, for highly dynamic processes GI is less applicable, if several sub-images are acquired to perform the reconstruction of the different contrast types[6,7].

To realize single-exposure acquisition without moving optical components, Hartmann sensors can be used. Here, the X-ray beam is propagated through individual sub-apertures in a fully absorbing plane leading to a 2D array of beamlets[1,8,9]. This method, however, exhibits low overall efficiency due to the unfavorable area fraction of the sub-apertures, preventing its use for applications at low flux. The efficiency can be increased by using an array of lenslets instead of simple apertures, where most of the incoming flux is focused onto small spots on the detector, analogously to a Shack-Hartmann sensor for visible light[7]. In spite, the image formation process remains unmodified.

X-ray lenses, forming cavities in a suitable material, whose refractive index in the X-ray range is normally below 1, are used since years. Starting from cylindrical lenses for line foci[10] or crossed cylinders[11] and spherical lenses[12] for a spot focus, these have been developed further to a paraboloid shape with increasing focusing efficiency[11–14]. To obtain focal distances in the centimeter range, several single lenses are stacked to obtain compound refractive lenses (CRL)[12]. Also, 1D arrays of line foci lenses have been produced[15]. Following the proposal in[16] by Piestrup only few realisations of 2D lens arrays have been reported to date[7,17].

Here we demonstrate how scalable 2D lens arrays can be produced using standard polyimide foils. A Compound Array Refractive Lens is presented, with 99x99 spots and a pitch of 65 µm covering an area of 6.5x6.5 mm^2 and a focal length of about 85 cm at an X-ray energy of 9 keV. This array is used to retrieve absorption, phase and scattering contrast during pulsed laser ablation in liquid (PLAL) with microsecond temporal resolution. Nanoparticles (NP) are detected through the scattering channel, aided by decorrelation of the absorption channel. The process of residue-free NP synthesis by PLAL is a hierarchical process involving several length and time scales[18,19] from the laser-matter interaction time up to ripening of NPs on a late stage[20,21]. Therefore a correlation between nanoscale distribution and macroscale dynamics is very important[22,23]. Multi-contrast imaging with a Shack-Hartmann sensor based on compound lens arrays represents a promising tool to investigate this phenomenon.

The CARL consists of a stack of polyimide foils, of which each possesses a 2D array of plane-concave single lenses, as proposed earlier[16]. We produce a 2D lens array of each foil by an embossing process. A steel needle serves as a stamp that is shaped into a paraboloid cone (apex radius 25 µm). This shape reduces spherical aberrations[11]. The needle is mounted onto a hexapod (PI miCos HP-550), in order to precisely position it with respect to the foil. Foils of commercial Kapton® with thickness of 75 µm are mounted onto a flat, electrically conductive plate. Alignment is aided by video microscopy and measuring the conductivity between the needle and the conducting support. The lens array is produced by starting with a position in the center and continuing in a spiral order

[a)] Electronic mail: anton.plech@kit.edu

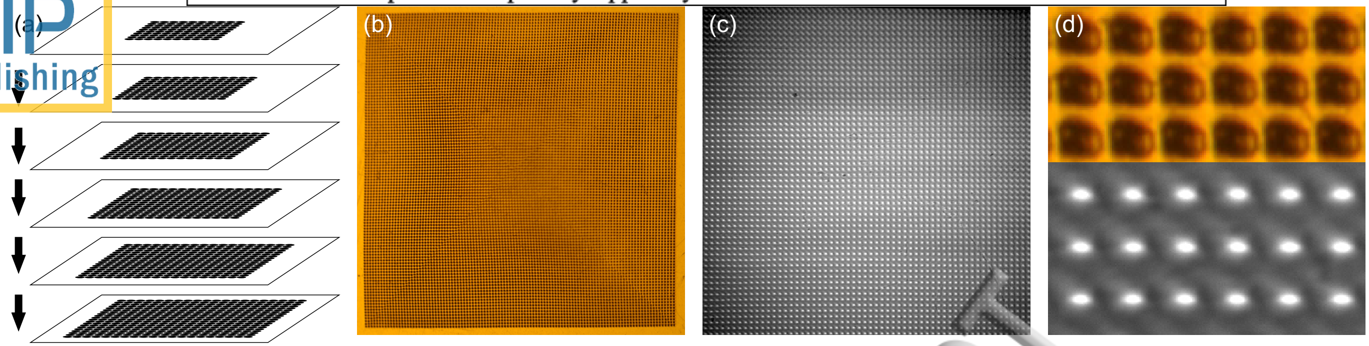

FIG. 1. (a) Scheme of the fabrication of the compound array refractive lens by first a sequential embossing of lenses in foils and later successive stacking of these foils and fixation. (b) Image of a single foil displaying the uniformity of the array. The diagonal distortion is linked to the pyramidal foil bending. (c) Detector image of the focal plane of six stacked foils with X-ray illumination. (d) Detailed images of (b) and (c).

around the first position with an indent depth of 20 µm. Thus, the plastic strain is symmetrically shifted towards the outer array parts. Due to this plastic flow in the embossing process a slight pyramidal shape develops in the lens array (visible in Fig. 1 (b) as a slight defocusing of the center in the optical micrograph and a hint of pyramidal facets). The elevation of the pyramid is estimated to be less than 400 µm.

The array size of successive foils in the final stack is enlarged by one line of lenses each, starting with an array of 99x99 lenses. This aids the alignment of the semi-transparent foils under the microscope. Starting with the largest lens array the next-in-line array is positioned precisely on top by a manual goniometer and glued in place (see Fig. 1 (a)). A slight (< 5 µm) misalignment of lenses in a CRL is mainly changing the absolute transmission of the CRL[24,25], which is uncritical in our case.

The characterization of the CARL and multi-contrast imaging of the ablation process were performed at the synchrotron at KIT (Karlsruhe, Germany), at the tomography instrument TOPO-TOMO[26]. For characterization and PLAL imaging monochromatic X-rays at 9 keV (bandwidth 2%) and a white beam (central energy 15 keV, filtered by 0.2 mm of Al) were used, respectively. X-rays were detected by a CMOS camera (Andor Neo with 10 µm LsO:TB and PCO.dimax with 50 µm LuAg:Ce scintillator for focus measurement and PLAL, respectively). Corrections for dark current and flat-field distortions were performed (illumination without X-rays and 10 images before laser action, respectively). This setup is illustrated in Fig. 2. The X-rays coming from the synchrotron were concentrated into the beamlets by the CARL (see Fig. 1 (c)). The sample was placed between the CARL and the detector. Technically, it is also possible to place the sample in front of the CARL as usually done in GI[27]. Here we need a short distance between the sample and the detector for setting the length scale in scattering contrast. The CARL was placed at a distance to the detector, which corresponded to the calculated focal length for 15 keV. Note that the point of tightest focus was slightly broadened due to the usage of a filtered white beam. Time resolution was gained by operating the active-pixel camera (PCO.dimax) with a frame rate of 10 kHz and 30 µs exposure per frame. A fourfold interleaving of records with shifted time delay between laser and camera results in an effective frame rate of 40 kHz. A delay generator (Research Instruments, DG535) controlled the delay between laser and camera.

The ablation process was performed in a 3D-printed flow chamber. The chamber design and functionality was described elsewhere[19]. In brief, the chamber had a rectangular reaction volume of 0.5 ml with channels providing an optimized water flow. The laser was focused onto the target by a lens, which also acted as a chamber seal. The side walls were sealed by Kapton® foils, allowing for X-ray transmission. As target a Zn wire (1 mm, Advent, 99.99%) was used and continuously transported (perpendicular to laser and X-ray beam) to obtain a clean surface spot for each individual laser shot. The wire was suspended in water being clamped on each sides 5 mm away from the ablation spot. The laser was a Nd:YAG laser (wavelength 1064 nm, Continuum Minilite I) with 10 mJ pulse energy. An average over 500 shots was acquired for each distance, taking advantage of the repeatability of the process.

The general image and contrast formation have been described in earlier publications[2,7,28]. The overall performance of the different optical elements depends on the beam structuring (visibility) and on the retrieval algorithm[29]. The CARL creates a spot for each CRL stack on the detector. The change of each of these spots by the sample in intensity, position and width corresponds to absorption, differential phase and scattering, respectively. It should be noted that the distinction between phase and scattering contrast is interdependent of each other and reflects on the geometry and size of the objects in the experimental setup[30]. Also, crosstalk from absorption to scattering contrast is of importance for a proper data analysis[31].

We used 2D-Gaussian fit[7,9,32] for the estimation of the

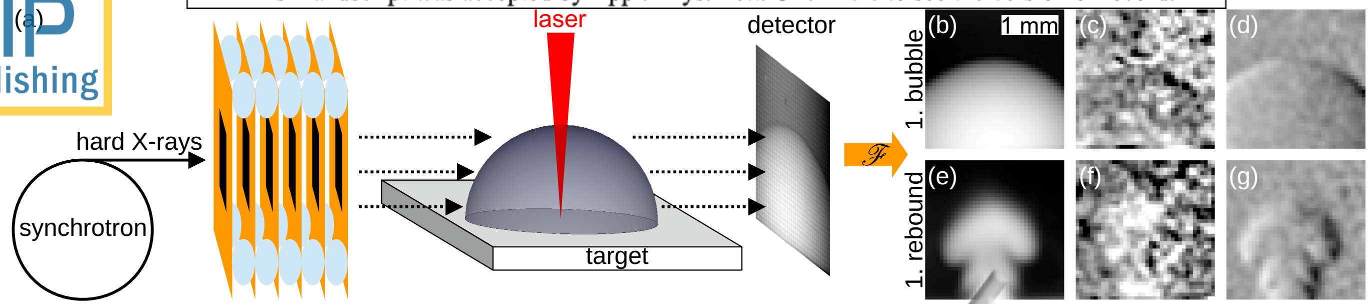

FIG. 2. (a) Setup: X-rays from the synchrotron are focused into an array of beamlets by the CARL before intersecting the sample and being detected by a (fast) X-ray image detector. From the relative changes of intensity, position and width the different contrasts are reconstructed. Two sets of images at the large distance: (b)-(d) for the first cavitation bubble and (e)-(f) for the first rebound. (b) and (e) show the transmission (higher transmission = brighter), (c) and (f) the scattering contrast (higher scattering = brighter) and (d) and (g) the lateral differential phase contrast.

height, position and width of the spots (for more details see supplementary material, section I A) for the CARL characterization. It is also possible to retrieve absorption, differential phase and scattering contrasts from Fourier analysis, assuming that the spots reside on a quadratic array with equal spacing[1,2,28,33]. The ablation dynamics have been analysed this way due to the higher robustness with noisy data and reduced calculation time. In brief, the image is Fourier transformed, specific harmonic regions are cropped and back transformed. The central harmonic represents the transmission, higher harmonics the scattering in specific directions and the complex angle of higher harmonics the differential phase. As the higher harmonics are a superposition of absorption and scattering a normalization is necessary. For more details see supplementary material section I B.

As the ablation process is highly dynamic a microsecond time resolution is needed. Averaging of the recorded sequences over 500 subsequent laser shots was necessary in order to improve the signal-to-noise ratio. As the NP do scatter isotropically, averaging over the three directional scattering channels in (x,y) equalling (1,0), (0,1) and (1,1) of first order was performed. Crosstalk between absorption and scattering was removed by a linear decorrelation (see supplementary material section I C).

The focal distance of a plan-concave CRL[10] is $f = R/(N \cdot \delta)$ with R, N and δ being the radius of curvature at the apex, number of stacked lenses and the decrement of the index of refraction of the lens material. With an approximate radius of curvature of (25 ± 5) µm and $\delta = 3.76 \cdot 10^{-6}$ for polyimide at 9 keV, the expected focal distance is $f_{theo} = (110 \pm 20)$ cm.

As shown in Fig. 3 (a) the position of minimal spot size (for a region of 20x20 spots, calculated by polynomial fit of order 2) is at 76 and 96 cm for x- and y-direction, respectively. This is in fair agreement with the expected value. The beamlet intensity also peaks at 78 cm.

The slight difference in spot size in the two directions originates from the imaging of the synchrotron source size by the lenses. Placed at a bending magnet of the ring, the horizontal source size (with 2 mm primary slit opening)

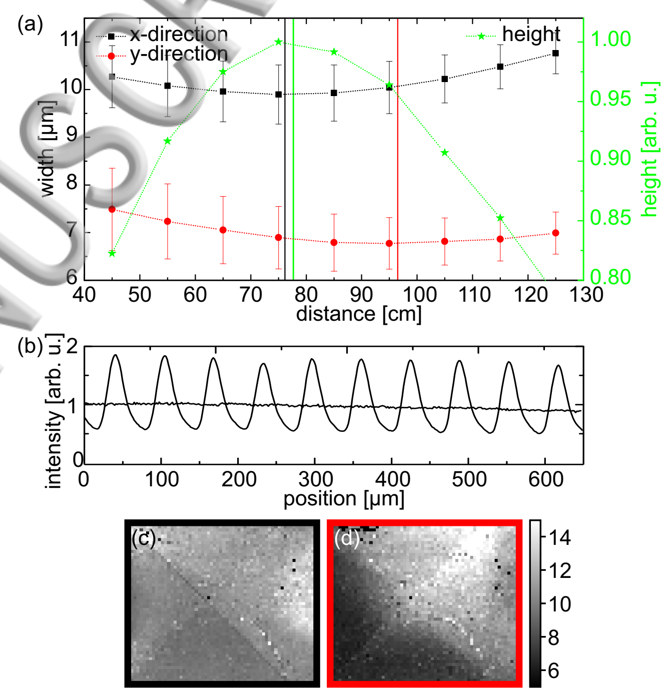

FIG. 3. (a) Width and height of X-ray spots as function of distance between lens array and detector from an average of 20x20 spots (left bottom). Vertical lines mark the tightest spot positions for the two directions and the maximum height. (b) Intensity along a line of beamlets at a distance of 85 cm, with the incoming beam (flat line) and the beam after the lens array (curved line). (c) and (d) show the width of the spots in x- and y-direction over the CARL array at 85 cm.

is larger than in vertical direction (0.2 mm). The finite source size may also be the reason for the rather flat distribution of focal spot size versus distance and the apparently decreased focus length. The geometric focus competes with the demagnification of source size at a relatively shorter distance.

Fig. 3 (c) and (d) display the spot width in x- and y-direction of 62x53 spots at a distance of 85 cm, with sufficient uniformity across the lens array. Again, the pyra-

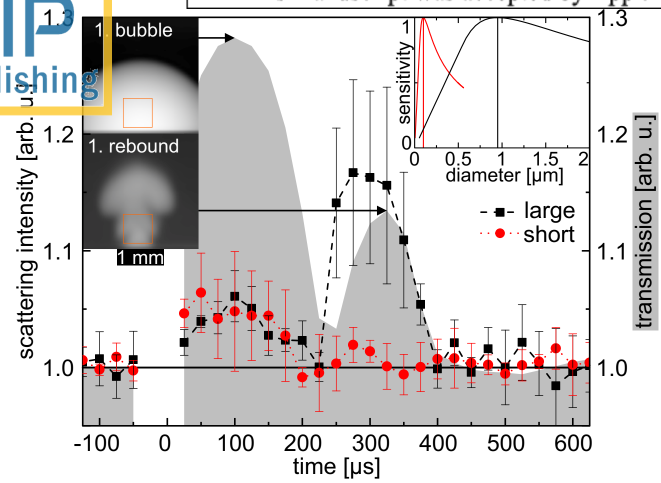

FIG. 4. Temporal evolution of the scattering signal (symbols) during laser ablation for short and large sample-detector distance. The insets on the left show two radiographs at selected delays with the position the scattering analysis. The inset on the right plots the normalized sensitivity distributions for both distances.

midal distortion is slightly visible. The average width for the whole CARL is in x-direction (11 ± 2) µm and in y-direction (10 ± 3) µm. This spot size is mainly limited by the source size at a demagnification of 40. Therefore slight imperfections in the CARL, such as stacking shifts and the pyramidal distortions contribute less than the source size effect. Additionally, contrast retrieval compares images with and without sample in order to derive relative changes. The absolute value of focal spot size defines visibility and thus the absolute sensitivity. Fig. 3 (b) shows a line section in x-direction over 10 spots. The intensity modulation shows a visibility of around 0.4, comparable to typical GI setups[34]. The visibility may be further increased by forming concave lenslets that extend to the edge of the unit cell, where right now considerable intensity remains unmodified due to low absorption in Kapton.

The utility of this setup is demonstrated by imaging the temporal structure evolution in PLAL. Energy deposited by the pulsed laser in the metal target and water phase for nanosecond laser pulses[35] leads to spallation of zinc into the water phase. At the same time a cavitating vapor bubble is induced. The latter grows to a millimeter size within some 100 microseconds before collapsing and eventually forming rebouncing secondary bubbles. While it is known that most of the ablated nanoparticulate material is contained in this bubble, details of the interaction between bubble and NPs, such as redeposition and agglomeration are still under investigation[19,36]. Typical X-ray radiographs (transmission contrast) are displayed in Fig. 4 as inset (see supplementary material for a video with all contrasts). The fully extended (hemispherical) first bubble as well as the detached first rebound structure are found at delays of 100 µs and 325 µs, respectively. The latter is of complicated nature, as it does not seem to be a homogeneous cavity[37]. Fig. 4 plots the values of the scattering signals inside the bubble as function of delay after laser excitation both for a short (4.4 cm) and large (40 cm) sample-detector distance. The transmission contrast is overlaid as grey area.

Earlier SAXS measurements have shown mostly two size levels of produced NPs, one with diameters of approximately 10 nm and one with diameters larger than 40 nm[18,19,22,23] in silver or gold. Zinc ablation produces larger particles (between 10 and 70 nm). Scattering contrast shows up where a sufficient concentration of structures within the sensitivity interval are located.

The peak sensitivity for both sample-detector distances changes from 100 nm for the short to 950 nm for the large distance[38]. The normalized sensitivities are shown as inset in Fig. 4. It should be mentioned that the absolute sensitivity for the short distance is lower than that for the large distance. As consequence, smaller structures remain visible for an increase in detector distance, as seen earlier[39–41]. Large structures only appear with the larger distance.

A clear difference in the signals for the short and large sample-detector distance is observed. Within the first bubble (0-250 µs delay) the signal of the short distance is higher compared to the first rebound (250-400 µs). This is in contrast to the signal evolution at the large sample-detector distance. Here, the signal within the first rebound is boosted considerably. Both signals return to almost 0 after the bubbles have vanished. The difference in size sensitivity allows identifying the signal at the short distance of being related to the ablated NPs within the bubble, while at the large distance the sensitivity on larger structures favors the notion of emerging microbubbles. Additionally, agglomerated NPs may add to the signal at large distance. This is in line with findings in optical stroboscopy and X-ray radiography[37], where the first rebound and in particular the bubble stem were optically opaque and seemingly not homogeneous, showing micrometer scale metastable permanent gas bubbles[42].

The multi-contrast and in particular scattering imaging allows for the identification of nanoscale features during X-ray imaging. While the integral scattering signal does not allow resolving different sizes directly, a variation of sample-detector distance can coarsely discriminate different size fractions.

We demonstrated a facile route for fabricating a 2D array of X-ray lenses by sequential stamping into a polymer foil. We realized an area of 99x99 lenses and 6.5x6.5 mm^2, respectively. The compound produces a focal length of 85 cm. Lateral size is further scalable, the pattern is easily changeable and the focal distance can be changed by the needle shape or further stacking. This CARL allows for the simultaneous assessment of absorption, differential phase and scattering in single-exposure X-ray measurements. By using a CARL the local flux density is increased compared to the use of Hartmann masks leading to decreased exposure times. The increased flux density allows for a better access to the fast process of PLAL. It is shown that by changing the sample-detector distance the setup is sensitive to different sizes of scattering objects.

By using the differential phase the CARL can also be used as a Shack-Hartmann sensor for hard X-rays (SHARX)[7]. Further improvements in the fabrication can be obtained by stamping with needles of better defined shape and needle arrays. A central parameter to improve is the visibility contrast which can be achieved by higher fill factors in the lens plane. To improve the scattering sensitivity further one could also produce different pitches in x- and y-direction to gain results of different sensitivities within one measurement[41].

See supplementary material for (i) the detailed description of the multi-contrast retrieval, (ii) multi-contrast images of the first rebound and (iii) a video of the important contrasts of the ablation process.

Provision of beam time at ANKA is acknowledged. We acknowledge T. Müller for support at the beamline and the German Research Foundation DFG through grant PL 325/8-1.

[1]H. H. Wen, E. E. Bennett, R. Kopace, A. F. Stein, and V. Pai, Opt. Lett. **35**, 1932 (2010).
[2]H. Wen, E. E. Bennett, M. M. Hegedus, and S. Carroll, IEEE Trans. Med. Imag. **27**, 997 (2008).
[3]A. Velroyen, A. Yaroshenko, D. Hahn, A. Fehringer, A. Tapfer, M. Müller, P. B. Noël, B. Pauwels, A. Sasov, A. Yildirim, O. Eickelberg, K. Hellbach, S. D. Auweter, F. G. Meinel, M. F. Reiser, M. Bech, and F. Pfeiffer, EBioMedicine **2**, 1500 (2015).
[4]M. Bech, A. Tapfer, A. Velroyen, A. Yaroshenko, B. Pauwels, J. Hostens, P. Bruyndonckx, A. Sasov, and F. Pfeiffer, Sci. Rep. **3**, 3209 (2013).
[5]F. Pfeiffer, M. Bech, O. Bunk, P. Kraft, E. F. Eikenberry, C. Brönnimann, C. Grünzweig, and C. David, Nat. Mater. **7**, 134 (2008).
[6]S. A. McDonald, F. Marone, C. Hintermüller, G. Mikuljan, C. David, F. Pfeiffer, and M. Stampanoni, J. Synchrotron Rad. **16**, 562 (2009).
[7]T. dos Santos Rolo, S. Reich, D. Karpov, S. Gasilov, D. Kunka, E. Fohtung, T. Baumbach, and A. Plech, (2018), arXiv:1802.10045.
[8]K. S. Morgan, D. M. Paganin, and K. K. W. Siu, Opt. Express **19**, 19781 (2011).
[9]F. A. Vittoria, M. Endrizzi, P. C. Diemoz, A. Zamir, U. H. Wagner, C. Rau, I. K. Robinson, and A. Olivo, Sci. Rep. **5**, 16318 (2015).
[10]A. Snigirev, V. Kohn, I. Snigireva, and B. Lengeler, Nature **384**, 49 (1996).
[11]B. Lengeler, J. Tümmler, A. Snigirev, I. Snigireva, and C. Raven, J. Appl. Phys. **84**, 5855 (1998).
[12]B. Lengeler, C. G. Schroer, J. Tümmler, B. Benner, M. Richwin, A. Snigirev, I. Snigireva, and M. Drakopoulos, J. Synchrotron Rad. **6**, 1153 (1999).
[13]E. Kornemann, O. Márkus, A. Opolka, T. Zhou, I. Greving, M. Storm, C. Krywka, A. Last, and J. Mohr, Opt. Express **25**, 22455 (2017).
[14]S. Gasilov, A. Mittone, T. dos Santos Rolo, S. Polyakov, S. Zholudev, S. Terentyev, V. Blank, A. Bravin, and T. Baumbach, J. Synchrotron Rad. **24**, 1137 (2017).
[15]M. Lyubomirskiy, I. Snigireva, V. Kohn, S. Kuznetsov, V. Yunkin, G. Vaughan, and A. Snigirev, J. Synchrotron Rad. **23**, 1104 (2016).
[16]M. A. Piestrup, "X-ray and neutron imaging," (2003).
[17]V. P. Nazmov, J. Mohr, H. Vogt, R. Simon, and S. Diabaté, J. Micromech. Microeng. **24**, 075005 (2014).
[18]S. Ibrahimkutty, P. Wagener, A. Menzel, A. Plech, and S. Barcikowski, Appl. Phys. Lett. **101**, 103104 (2012).
[19]S. Ibrahimkutty, P. Wagener, T. dos Santos Rolo, D. Karpov, A. Menzel, T. Baumbach, S. Barcikowski, and A. Plech, Sci. Rep. **5**, 16313 (2015).
[20]H. Zeng, X. W. Du, S. C. Singh, S. A. Kulinich, S. Yang, J. He, and W. Cai, Adv. Funct. Mater. **22**, 1333 (2012).
[21]D. Zhang, B. Gökce, and S. Barcikowski, Chem. Rev. **117**, 3990 (2017).
[22]P. Wagener, S. Ibrahimkutty, A. Menzel, A. Plech, and S. Barcikowski, Phys. Chem. Chem. Phys. **15**, 3068 (2013).
[23]A. Letzel, B. Gökce, P. Wagener, S. Ibrahimkutty, A. Menzel, A. Plech, and S. Barcikowski, J. Phys. Chem. C **121**, 5356 (2017).
[24]H. R. Beguiristain, J. T. Cremer, M. A. Piestrup, R. H. Pantell, C. K. Gary, and J. Feinstein, in *Proc. SPIE*, Vol. 4144, edited by C. A. MacDonald and A. M. Khounsary (2000) pp. 155–164.
[25]R. H. Pantell, J. Feinstein, H. R. Beguiristain, M. A. Piestrup, C. K. Gary, and J. T. Cremer, Rev. Sci. Instrum. **72**, 48 (2001).
[26]T. dos Santos Rolo, A. Ershov, T. van de Kamp, and T. Baumbach, Proc. Natl. Acad. Sci **111**, 3921 (2014).
[27]T. Donath, M. Chabior, F. Pfeiffer, O. Bunk, E. Reznikova, J. Mohr, E. Hempel, S. Popescu, M. Hoheisel, M. Schuster, J. Baumann, and C. David, J. Appl. Phys. **106**, 054703 (2009).
[28]H. Wen, E. E. Bennett, M. M. Hegedus, and S. Rapacchi, Radiology **251**, 910 (2009).
[29]F. A. Vittoria, G. K. N. Kallon, D. Basta, P. C. Diemoz, I. K. Robinson, A. Olivo, and M. Endrizzi, Appl. Phys. Lett. **106**, 224102 (2015).
[30]T. Koenig, M. Zuber, B. Trimborn, T. Farago, P. Meyer, D. Kunka, F. Albrecht, S. Kreuer, T. Volk, M. Fiederle, and T. Baumbach, Phys. Med. Biol. **61**, 3427 (2016).
[31]S. Kaeppler, F. Bayer, T. Weber, A. Maier, G. Anton, J. Hornegger, M. Beckmann, P. A. Fasching, A. Hartmann, F. Heindl, T. Michel, G. Oezguel, G. Pelzer, C. Rauh, J. Rieger, R. Schulz-Wendtland, M. Uder, D. Wachter, E. Wenkel, and C. Riess, "Signal decomposition for x-ray dark-field imaging," in *MICCAI 2014, Part I*, edited by P. Golland, N. Hata, C. Barillot, J. Hornegger, and R. Howe (Springer International Publishing, 2014) pp. 170–177.
[32]M. Endrizzi, P. C. Diemoz, T. P. Millard, J. Louise Jones, R. D. Speller, I. K. Robinson, and A. Olivo, Appl. Phys. Lett. **104**, 024106 (2014).
[33]Y. Liu, B. Ahr, A. Linkin, G. J. Diebold, and C. Rose-Petruck, Opt. Lett. **36**, 2209 (2011).
[34]C. David, B. Nöhammer, H. H. Solak, and E. Ziegler, Appl. Phys. Lett. **81**, 3287 (2002).
[35]S. Reich, P. Schönfeld, A. Letzel, S. Kohsakowski, M. Olbinado, B. Gökce, S. Barcikowski, and A. Plech, ChemPhysChem **18**, 1084 (2017).
[36]S. Reich, P. Schönfeld, P. Wagener, A. Letzel, S. Ibrahimkutty, B. Gökce, S. Barcikowski, A. Menzel, T. dos Santos Rolo, and A. Plech, J. Colloid Interface Sci. **489**, 106 (2017).
[37]S. Reich, J. Göttlicher, A. Letzel, B. Gökce, S. Barcikowski, T. dos Santos Rolo, T. Baumbach, and A. Plech, Appl. Phys. A **124**, 71 (2018).
[38]S. K. Lynch, V. Pai, J. Auxier, A. F. Stein, E. E. Bennett, C. K. Kemble, X. Xiao, W.-K. Lee, N. Y. Morgan, and H. H. Wen, Appl. Opt. **50**, 4310 (2011).
[39]M. Strobl, Sci. Rep. **4**, 7243 (2014).
[40]F. Prade, A. Yaroshenko, J. Herzen, and F. Pfeiffer, EPL **112**, 68002 (2015).
[41]A. F. Stein, J. Ilavsky, R. Kopace, E. E. Bennett, and H. Wen, Opt. Express **18**, 13271 (2010).
[42]S. Kohsakowski, A. Santagata, M. DellAglio, A. de Giacomo, S. Barcikowski, P. Wagener, and B. Gökce, Appl. Surf. Sci. **403**, 487 (2017).

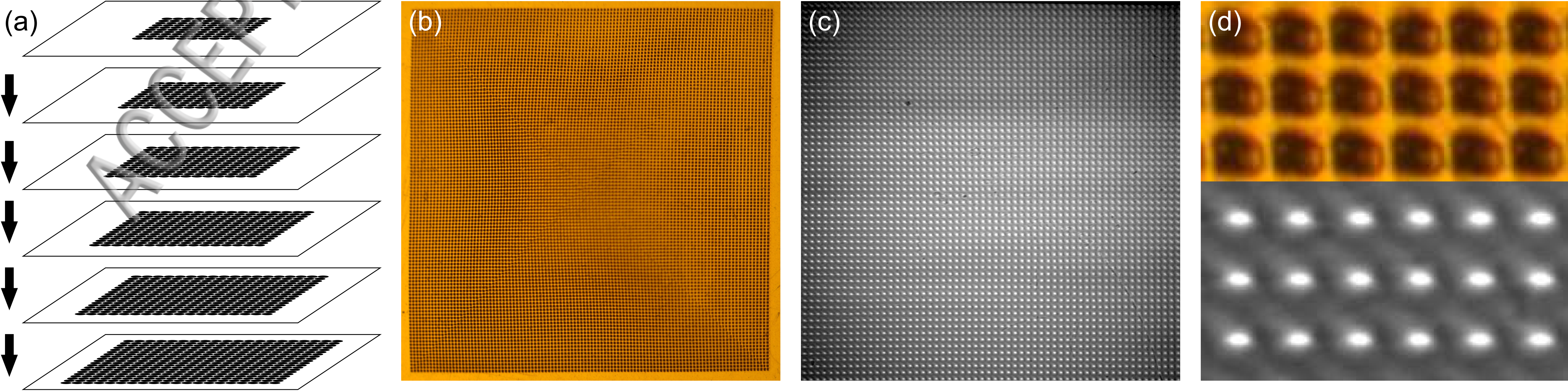
(a)
(b)
(c)
(d)

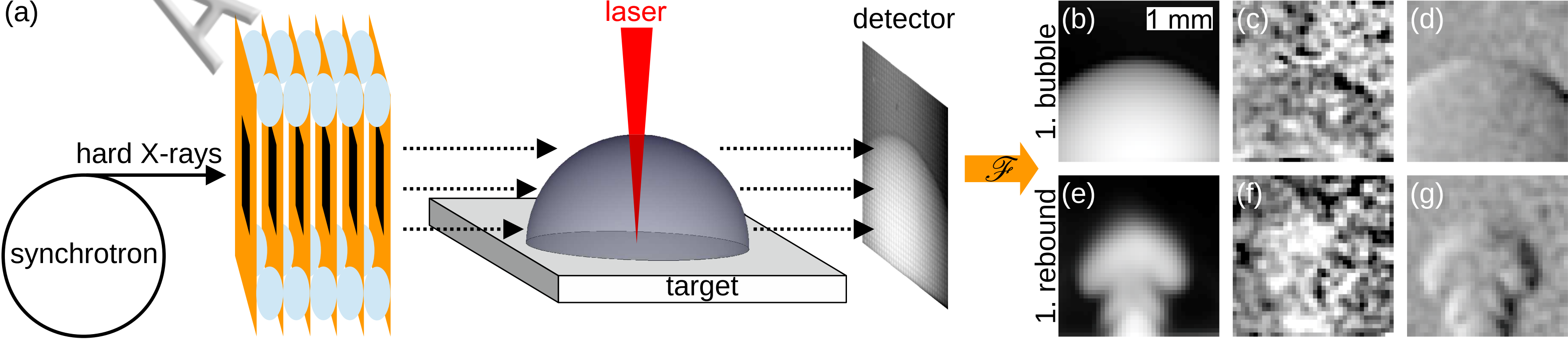

(a)
laser
detector
hard X-rays
synchrotron
target
(b)
1 mm
(c)
(d)
1. bubble
(e)
(f)
(g)
1. rebound

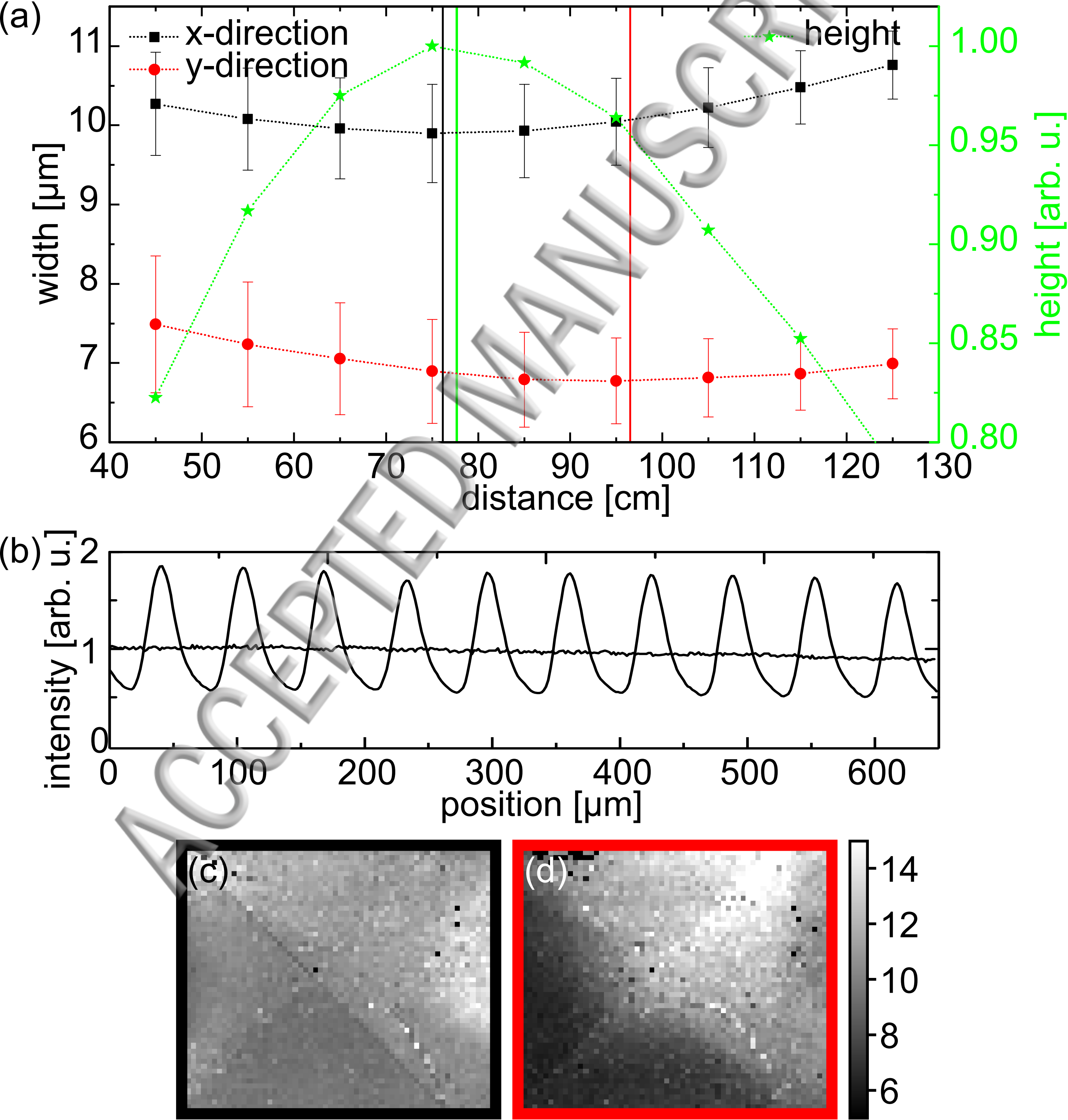

(a)
x-direction
y-direction
height
width [µm]
height [arb. u.]
distance [cm]
(b)
intensity [arb. u.]
position [µm]
(c)
(d)

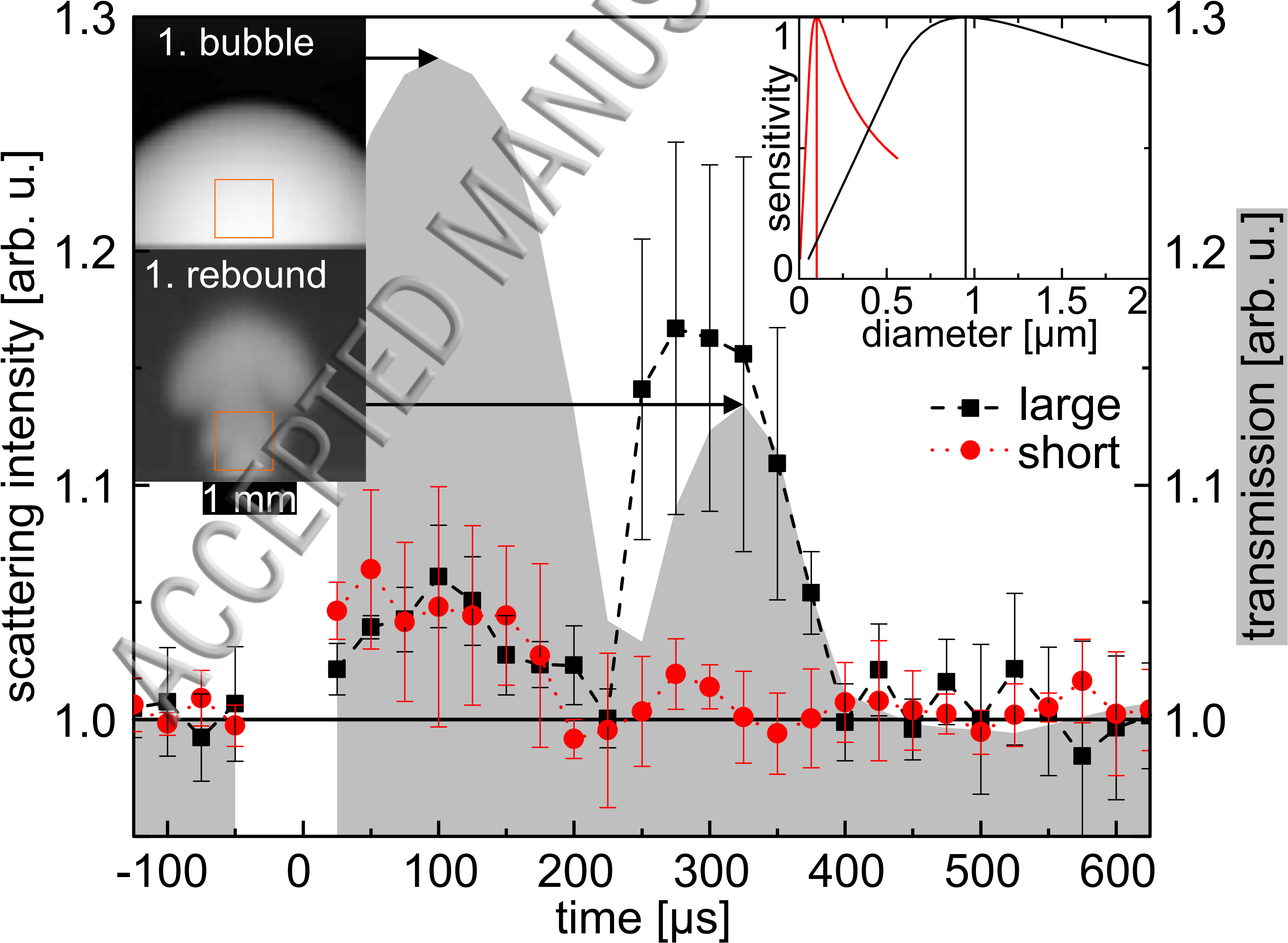
1. bubble
1. rebound
1 mm
sensitivity
diameter [µm]
large
short
scattering intensity [arb. u.]
transmission [arb. u.]
time [µs]
ACCEPTED MANUSCRIPT